

Analytical gradients and nonadiabatic couplings for the state-average density matrix renormalization group self-consistent field method

Leon Freitag,^{1, a)} Yingjin Ma,^{2, 3} Alberto Baiardi,¹ Stefan Knecht,¹ and Markus Reiher^{1, b)}

¹⁾ *ETH Zürich, Laboratorium für Physikalische Chemie, Vladimir-Prelog-Weg 2, 8093 Zürich, Switzerland*

²⁾ *Department of High Performance Computing, Computer Network Information Center, Chinese Academy of Sciences, Beijing 100190, China*

³⁾ *Center of Scientific Computing Applications & Research, Chinese Academy of Sciences, Beijing 100190, China*

(Dated: May 4, 2019)

We present analytical gradients and nonadiabatic couplings for a state-average density matrix renormalization group self-consistent-field (SA-DMRG-SCF) wavefunction. Our formalism follows closely the state-average complete active space self-consistent-field (SA-CASSCF) *ansatz*, which employs a Lagrangian, and the corresponding Lagrange multipliers are obtained from a solution of the coupled-perturbed CASSCF (CP-CASSCF) equations. We introduce a definition of the MPS Lagrange multipliers based on the mixed-canonical form of the MPS, such that the sweep procedure is avoided in the solution of the CP-CASSCF equations. We employ our implementation for the optimization of a conical intersection in 1,2-dioxetanone, where we are able to fully reproduce the SA-CASSCF result up to arbitrary accuracy.

I. INTRODUCTION

Multiconfigurational methods are tailored for molecular systems exhibiting strong electronic correlation, as found in many transition metal complexes,^{1–9} bond dissociation processes and excited electronic states.^{6,10–13} Excited electronic states are of key importance for photoinduced phenomena, including light-matter interaction with DNA,^{14–16} light harvesting, photocatalysis and artificial photosynthesis,^{17–20} as well as photodynamic cancer therapy.^{21–24}

The majority of modern multiconfigurational methods are based on the complete active space self-consistent field (CASSCF) method,^{25–28} which, however, scales exponentially with the number of active orbitals, and as such, has been effectively limited to about 18 active orbitals.²⁹ Only recently, this limit has been raised to 20 orbitals through massive parallelization.³⁰ One successful remedy to the exponential scaling problem of CASSCF has been the quantum chemical density matrix renormalization group (DMRG).^{31–50} DMRG was originally introduced by White^{51,52} to solid state physics in 1992, but has found numerous applications in quantum chemistry since then.^{53–70} Combined with the self-consistent field orbital optimization (DMRG-SCF),^{71–75} the method is able to approximate a CASSCF wavefunction to arbitrary accuracy with polynomial scaling³³ by reducing the size of the configurational space amidst the optimization of a so-called matrix product state (MPS) wavefunction,^{76,77} therefore allowing for much larger active spaces than traditional CASSCF.

Many problems in quantum chemistry tackled by DMRG and DMRG-SCF^{78–86} require only the calculation of electronic energies and properties. However, in photochemistry, many phenomena rely on optimizing excited state structures, locating conical intersections and potential energy surface crossings or on performing ab-initio molecular dynamic simulations. These tasks require not only the efficient calculation of the energy of the ground and excited electronic states, but also of energy gradients and nonadiabatic couplings.

The most efficient way to calculate gradients is through the derivation of analytical expressions, as originally introduced by Pulay.^{87–90} Accordingly, an analytical formulation for nonadiabatic couplings has been introduced by Yarkony and co-workers.⁹¹ Analytical gradients are easily evaluated for a fully variationally-optimized wavefunction with the help of the Hellmann-Feynman theorem.^{92,93} Single-state multiconfigurational self-consistent-field (MCSCF) wavefunctions are fully variationally optimized, and hence the state-specific CASSCF analytical gradient formulation⁹⁴ has appeared shortly after CASSCF has been introduced. The same holds true for single-state DMRG-SCF gradients, which have been introduced by Liu et al.⁹⁵ and Hu and Chan⁹⁶ and have found several applications in ground and excited state structure optimizations^{95–97} and resonance Raman spectra.⁹⁸

However, state-specific MCSCF methods have disadvantages, especially when applied to excited states. First, a specific state may not be tracked easily. For example, the so-called *root flipping*, i.e. a change of the excited state order during orbital optimization may occur (although the problem can be partially alleviated if the state with the maximum overlap to the state of interest is followed during the optimization).^{96,98} Second, a state-specific optimization does not guarantee orthogonality of the individually optimized states to each other that

^{a)} Electronic mail: leon.freitag@phys.chem.ethz.ch (corresponding author)

^{b)} Electronic mail: markus.reiher@phys.chem.ethz.ch (corresponding author)

greatly simplifies the calculation of excited state properties and, in particular, of nonadiabatic couplings.^{91,99,100}

One possible remedy for the disadvantages of the state-specific optimization is the state-average MC-SCF *ansatz*,^{101–103} where several states are optimized simultaneously using a single set of molecular orbitals (MOs) which yields the best average energy of the states of interest. In the state-average *ansatz*, the root flipping problem does not occur¹⁰¹ and the states are necessarily orthogonal. However, with state-averaged MCSCF the gradient formalism loses its simplicity as the wavefunction is no longer fully variational. Nevertheless, the Hellmann-Feynman theorem can still be applied with the help of Lagrange multipliers^{104,105} that are obtained from the solution of the so-called coupled perturbed multiconfiguration self-consistent field (CP-MCSCF) equations.^{106,107} Stålring et al.¹⁰⁵ were the first to describe an SA-MCSCF analytic gradient formulation based on Lagrangians. Recently, Snyder et al.^{108,109} presented a GPU-based implementation of SA-CASSCF analytic gradients, following the work of Stålring et al.

Besides the gradients, the solution of the CP-MCSCF equations may also be used to calculate analytical nonadiabatic couplings in the SA-MCSCF formalism^{91,110} and for the second-order MCSCF orbital optimization procedure.^{111–119}

While the SA-CASSCF analytical gradient problem may be considered solved, this is not the case for state-average DMRG-SCF (SA-DMRG-SCF) analytical gradients. The main challenge that remains is an adequate definition of the Lagrange parameters for the gradient calculation. For traditional MCSCF wavefunctions one usually expresses these in the configuration basis, which is impractical for MPS wavefunctions optimized by DMRG due to the exponential growth of the number of configurations with the number of active orbitals. In our previous work on a second-order DMRG-SCF optimization scheme⁷⁵ we presented expressions for the MPS variational parameters and for the state-average Hessian. In this work we further develop the concept of variational parameters in an MPS wavefunction and employ them in a formulation for SA-DMRG-SCF analytical gradients and nonadiabatic couplings.

II. THEORY

As the SA-DMRG-SCF analytical gradient theory is closely related to SA-CASSCF analytical gradient theory, we will begin with a brief recap of the former. Further information can be found in Ref. 105 and especially the excellent paper by Snyder et al.¹⁰⁹. In particular, we adopt the notation of the latter work. The theory for the nonadiabatic couplings follows very closely the gradient theory – the differences between the two will be presented in Sec. II F.

A. Single-state CASSCF gradients

In single-state (or state-specific) CASSCF,¹²⁰ a wavefunction is defined as a linear combination of *configurations* $|\phi_I\rangle$:

$$|\Phi\rangle = \sum_I c_I |\phi_I\rangle \quad (1)$$

where the expansion coefficients c_I are called the *CI coefficients* and the configurations ϕ_I are chosen in such a way that they represent all possible excitations within a pre-defined active orbital space and do not include any excitations outside this space. The CI coefficients are obtained by diagonalizing the matrix of the non-relativistic electronic Hamiltonian

$$\hat{H} = \sum_{\substack{t,u \\ \tau}} \langle t|h|u\rangle a_{t\tau}^\dagger a_{u\tau} + \frac{1}{2} \sum_{\substack{t,u,v,w \\ \tau,\tau'}} (tu|vw) a_{t\tau}^\dagger a_{v\tau'}^\dagger a_{w\tau'} a_{u\tau} + E_{\text{core}} \quad (2)$$

in the basis of the configurations ϕ_I . Here, $\langle t|h|u\rangle$ and $(tu|vw)$ are the one- and two-electron integrals in a given orthonormal molecular orbital basis, respectively, and $a_{t\tau}^\dagger$ and $a_{t\tau}$ are creation and annihilation operators, respectively, for an orbital t and spin τ . E_{core} is the sum of the energy contribution from the inactive (doubly occupied) orbitals and the nuclear repulsion energy.

The wavefunction $|\Phi\rangle$ is a function of a set of variational parameters, namely the orbital rotational parameters $\boldsymbol{\kappa}$ and CI coefficients \mathbf{c}

$$|\Phi\rangle = \Phi(\boldsymbol{\kappa}, \mathbf{c}) \quad (3)$$

and is variationally optimized with respect to these parameters to yield a minimum single-state CASSCF energy

$$E^\Phi = \langle \Phi | \hat{H} | \Phi \rangle = \sum_{pq} \langle p|h|q\rangle \gamma_{pq} + \frac{1}{2} \sum_{pqrs} (pq|rs) \Gamma_{pqrs}, \quad (4)$$

with γ_{pq} and Γ_{pqrs} being the one- and two-particle reduced density matrices (RDMs), respectively. Since the optimized wavefunction $|\Phi\rangle$ is then fully variational with respect to all of its variational parameters, the energy gradient with respect to some perturbation x (e.g. nuclear displacement) may be calculated according to the the Hellmann-Feynman theorem:¹²¹

$$\begin{aligned} \frac{dE^\Phi}{dx} &= \left\langle \Phi \left| \frac{\partial \hat{H}}{\partial x} \right| \Phi \right\rangle \\ &= \sum_{pq} \frac{\partial \langle p|h|q\rangle}{\partial x} \gamma_{pq} + \frac{1}{2} \sum_{pqrs} \frac{\partial (pq|rs)}{\partial x} \Gamma_{pqrs}. \end{aligned} \quad (5)$$

B. SA-CASSCF analytical gradients

In SA-CASSCF, the wavefunction is determined by a variational optimization of the state-average energy of

several states Ψ

$$E^{\text{SA}} = \sum_{\Psi} \omega_{\Psi} E^{\Psi} = \sum_{\Psi} \omega_{\Psi} \langle \Psi | \hat{H} | \Psi \rangle \quad (6)$$

where ω_{Ψ} is the weight of a state Ψ , and the sum of all weights equals to 1. In this paper we will only consider a situation where all weights are equal, although Stålring et al.¹⁰⁵ and Snyder et al.¹⁰⁹ have also considered a non-equal-weights situation. Similarly to the single-state case, the state-average energy depends on a set of variational parameters

$$E^{\text{SA}} = E^{\text{SA}}(\boldsymbol{\kappa}, \mathbf{c}^1, \mathbf{c}^2, \dots, \mathbf{c}^n) \quad (7)$$

where $\boldsymbol{\kappa}$ are the orbital parameters and \mathbf{c}^{Ψ} are the CI parameters for state Ψ .

The optimization procedure ensures that the state-average energy is variational with respect to the orbital parameters, whereas the individual state-specific energies are variational only with respect to their own CI parameters, but not with respect to CI parameters of other states or orbital parameters.

$$\frac{\partial E^{\text{SA}}}{\partial \kappa_{pq}} = 0; \quad \frac{\partial E^{\Theta}}{\partial c_{\Theta I}} = 0; \quad \left. \frac{\partial E^{\Theta}}{\partial c_{\Phi I}} \right|_{\Phi \neq \Theta} \neq 0; \quad \frac{\partial E^{\Theta}}{\partial \kappa_{pq}} \neq 0; \quad (8)$$

Hence, the gradient cannot be calculated according to the Hellmann-Feynman theorem. Following the method of the Lagrange multipliers, we may construct a Lagrangian function L^{Θ} for state L^{Θ} starting from the energy expression (4)

$$L^{\Theta} = E^{\Theta} + \left(\sum_{pq} \bar{\kappa}_{pq}^{\Theta} \frac{\partial E^{\text{SA}}}{\partial \kappa_{pq}} - 0 \right) + \left(\sum_{\Psi I} \bar{c}_{\Psi I}^{\Theta} \frac{\partial E^{\text{SA}}}{\partial c_{\Psi I}} - 0 \right). \quad (9)$$

where $\bar{\kappa}_{pq}^{\Theta}$ and $\bar{c}_{\Psi I}^{\Theta}$ are the Lagrange multipliers corresponding to the orbital and CI parts, respectively. L^{Θ} is variational with respect to all parameters and, therefore, the Hellmann-Feynman theorem applies. The Lagrange multipliers can be obtained by exploiting the fact that the Lagrangian must be variational with respect to all of its parameters:

$$\frac{\partial L^{\Theta}}{\partial \bar{\kappa}_{pq}^{\Theta}} = \frac{\partial L^{\Theta}}{\partial \bar{c}_{\Psi I}^{\Theta}} = \frac{\partial L^{\Theta}}{\partial \kappa_{pq}} = \frac{\partial L^{\Theta}}{\partial c_{\Psi I}} = 0. \quad (10)$$

The first two equalities in Eq. (10) are trivially fulfilled and are equivalent to the definition of the constraints. Hence, the Lagrange multipliers are obtained from the other two equalities, yielding the *coupled perturbed* MC-SCF (CP-MCSCF) equations:

$$\frac{\partial L^{\Theta}}{\partial \kappa_{rs}} = \underbrace{\frac{\partial E^{\Theta}}{\partial \kappa_{rs}}}_{g_{rs}^{\Theta}} + \sum_{pq} \bar{\kappa}_{pq}^{\Theta} \underbrace{\frac{\partial^2 E^{\text{SA}}}{\partial \kappa_{pq} \partial \kappa_{rs}}}_{H_{pq,rs}^{\text{OO}}} + \sum_{\Psi I} \bar{c}_{\Psi I}^{\Theta} \underbrace{\frac{\partial^2 E^{\text{SA}}}{\partial c_{\Psi I} \partial \kappa_{rs}}}_{H_{\Psi I,rs}^{\text{CO}}} = 0, \quad (11)$$

$$\frac{\partial L^{\Theta}}{\partial c_{\Phi J}} = \sum_{pq} \bar{\kappa}_{pq}^{\Theta} \underbrace{\frac{\partial^2 E^{\text{SA}}}{\partial \kappa_{pq} \partial c_{\Phi J}}}_{H_{pq,\Phi J}^{\text{OC}}} + \sum_{\Psi I} \bar{c}_{\Psi I}^{\Theta} \underbrace{\frac{\partial^2 E^{\text{SA}}}{\partial c_{\Psi I} \partial c_{\Phi J}}}_{H_{\Psi I,\Phi J}^{\text{CC}}} = 0 \quad (12)$$

or in matrix form

$$\begin{pmatrix} \mathbf{H}^{\text{OO}} & \mathbf{H}^{\text{CO}} \\ \mathbf{H}^{\text{OC}} & \mathbf{H}^{\text{CC}} \end{pmatrix} \begin{pmatrix} \bar{\boldsymbol{\kappa}} \\ \bar{\mathbf{c}}^{\Theta} \end{pmatrix} = - \begin{pmatrix} \mathbf{g}^{\Theta} \\ 0 \end{pmatrix} \quad (13)$$

As can be seen from Eqs. (11) and (12), \mathbf{H} is the state-average Hessian matrix with its orbital-orbital (\mathbf{H}^{OO}), orbital-CI ($\mathbf{H}^{\text{OC}} = (\mathbf{H}^{\text{CO}})^T$) and CI-CI (\mathbf{H}^{CC}) components and \mathbf{g}^{Θ} is the state-specific orbital gradient for the state $|\Theta\rangle$.

After solving Eq. (13), we may construct the Lagrangian of Eq. (9), and calculate the gradient as follows:^{108,109}

$$\frac{dE^{\Theta}}{dx} = \sum_{pq} \frac{\partial \langle p|h|q\rangle}{\partial x} \gamma_{pq}^{\Theta,e} + \frac{1}{2} \sum_{pqrs} \frac{\partial (pq|rs)}{\partial x} \Gamma_{pqrs}^{\Theta,e} - \sum_{pq} X_{pq}^{\Theta,e} \frac{\partial S_{pq}}{\partial x} \quad (14)$$

The first two terms in Eq. (14) originate from the Hellmann-Feynman theorem. They seem identical to Eq. (5), but the one- and two-particle reduced density matrices have been replaced by their *effective* counterparts, $\gamma^{\Theta,e}$ and $\Gamma^{\Theta,e}$, that are given by:¹⁰⁹

$$\gamma^{\Theta,e} = \gamma^{\Theta} + \tilde{\gamma} + \bar{\gamma} \quad (15)$$

$$\Gamma^{\Theta,e} = \Gamma^{\Theta} + \tilde{\Gamma} + \bar{\Gamma}, \quad (16)$$

where $\tilde{\gamma}$ and $\bar{\gamma}$, as well as $\tilde{\Gamma}$ and $\bar{\Gamma}$ are the orbital and the CI contributions to the RDM, respectively:

$$\tilde{\gamma}_{pq} = \sum_{\Psi} \omega_{\Psi} \left(\sum_o \gamma_{oq}^{\Psi} \bar{\kappa}_{op}^{\Theta} - \gamma_{po}^{\Psi} \bar{\kappa}_{qo}^{\Theta} \right) \quad (17)$$

$$\bar{\gamma}_{pq} = \sum_{\Psi} 2\omega_{\Psi} \gamma_{pq}^{\Psi} \bar{c}_{\Psi}^{\Theta} \quad (18)$$

$$\tilde{\Gamma}_{pqrs} = \sum_{\Psi} \omega_{\Psi} \left(\sum_o \Gamma_{oqrs}^{\Psi} \bar{\kappa}_{op}^{\Theta} + \Gamma_{pors}^{\Psi} \bar{\kappa}_{oq}^{\Theta} + \Gamma_{pqos}^{\Psi} \bar{\kappa}_{or}^{\Theta} + \Gamma_{pqro}^{\Psi} \bar{\kappa}_{os}^{\Theta} \right) \quad (19)$$

$$\bar{\Gamma}_{pqrs} = \sum_{\Psi} 2\omega_{\Psi} \gamma_{pqrs}^{\Psi} \bar{c}_{\Psi}^{\Theta}. \quad (20)$$

Here $\gamma_{pq}^{\Psi\bar{c}_\Psi^\Theta}$ and $\Gamma_{pqrs}^{\Psi\bar{c}_\Psi^\Theta}$ are matrix elements of the one- and two-particle transition density matrices, respectively, between state Ψ and a state with the Lagrange parameters \bar{c}_Ψ^Θ as the CI coefficients. The last term in Eq. (14) is dubbed the ‘‘connection’’ term by Stalring et al.¹⁰⁵, and is evaluated from the effective CI Lagrangian and the derivative of the MO overlap matrix.^{108,109}

In practice, the CP-MCSCF equations (13) are not solved directly, since the cost of evaluating and storing the full Hessian is too large. Instead, iterative solvers such as the preconditioned conjugate gradient (PCG)¹⁰⁵ or the direct inversion of the iterative subspace (DIIS)¹⁰⁹ are employed, which only require the computation of matrix-vector products between the Hessian and a trial vector, i. e. $\mathbf{H}^{\text{OO}}\tilde{\kappa}^\Theta$, $\mathbf{H}^{\text{CO}}\tilde{\kappa}^\Theta$, $\mathbf{H}^{\text{CO}}\bar{c}^\Theta$ and $\mathbf{H}^{\text{CC}}\bar{c}^\Theta$, with $\tilde{\kappa}^\Theta$ and \bar{c}^Θ as trial vectors, which become equal to the corresponding Lagrange multipliers upon convergence. Although these quantities must be recalculated each iteration (by contrast, the Hessian needs to be calculated only once), one must store only a trial vector of size $n_\kappa + n_c$ instead of a full Hessian matrix. In addition, as will become evident in Section II E, evaluating certain matrix-vector products offers further computational advantages compared to evaluating the corresponding Hessian matrix elements.

C. DMRG and DMRG-SCF

Most commonly, DMRG for quantum chemistry is formulated in a matrix product state (MPS) formulation,^{76,77} where the wavefunction is represented as a matrix product state:

$$\begin{aligned} |\Psi\rangle &= \sum_{\sigma} \mathbf{M}^{\sigma_1} \mathbf{M}^{\sigma_2} \cdots \mathbf{M}^{\sigma_L} |\sigma\rangle \\ &= \sum_{\sigma} \sum_{a_1 \dots a_{L-1}} M_{1a_1}^{\sigma_1} M_{a_1 a_2}^{\sigma_2} \cdots M_{a_{L-1} 1}^{\sigma_L} |\sigma\rangle. \end{aligned} \quad (21)$$

Hence, the CI coefficients in Eq. (1) are encoded as a product of three-dimensional tensors \mathbf{M}^{σ_i} , $|\sigma\rangle = |\sigma_1, \dots, \sigma_L\rangle$ represents the *occupation number vector* in analogy to the configurations in Eq. (1), and L is the number of active orbitals. We may occasionally call the

$$\begin{aligned} \langle \Psi | \hat{H} | \Psi \rangle &= \sum_{\substack{a'_1, \dots, a'_{L-1} \\ a_1, \dots, a_{L-1} \\ \sigma \sigma'}} \left(M_{1a_1}^{\sigma_1} \cdots M_{a_{L-1} 1}^{\sigma_{L-1}} \right)^* \sum_{b_1, \dots, b_{L-1}} W_{1b_1}^{\sigma_1 \sigma'_1} \cdots W_{b_{L-1} 1}^{\sigma_{L-1} \sigma'_{L-1}} \left(M_{1a'_1}^{\sigma'_1} \cdots M_{a'_{L-1} 1}^{\sigma'_{L-1}} \right) \\ &= \sum_{\substack{a_{L-1} a'_{L-1} b_{L-1} \\ \sigma_L \sigma'_L}} M_{1a_{L-1}}^{\sigma_L \dagger} W_{b_{L-1} 1}^{\sigma_L \sigma'_L} \left(\cdots \sum_{\substack{a_1 a'_1 b_1 \\ \sigma_1 \sigma'_1}} M_{a_2 a_1}^{\sigma_2 \dagger} W_{b_1 b_2}^{\sigma_2 \sigma'_2} \left(\sum_{\sigma_1 \sigma'_1} M_{a_1 1}^{\sigma_1 \dagger} W_{1b_1}^{\sigma_1 \sigma'_1} M_{1a'_1}^{\sigma'_1} \right) M_{a'_1 a'_2}^{\sigma'_2} \cdots \right) M_{a'_{L-1} 1}^{\sigma'_L} \end{aligned} \quad (25)$$

where we have regrouped the multiplication by indices σ_i, σ'_i in the last step. We may now define *left boundaries* recursively as⁴³

quantities $M_{a_{l-1} a_l}^{\sigma_l}$ the elements of an *MPS tensor* at site (orbital) l . For the optimization, it is important to express the MPS in a *mixed-canonical form*⁴³ at an arbitrary site l :

$$|\Psi\rangle = \sum_{\sigma, a_1 \dots a_{L-1}} A_{1a_1}^{\sigma_1} \cdots A_{a_{l-2} a_{l-1}}^{\sigma_{l-1}} M_{a_{l-1} a_l}^{\sigma_l} B_{a_l a_{l+1}}^{\sigma_{l+1}} \cdots B_{a_{L-1} 1}^{\sigma_L} |\sigma\rangle, \quad (22)$$

where the tensors with elements $A_{a_{l-1} a_l}^{\sigma_l}$ are left-normalized and tensors with elements $B_{a_{l-1} a_l}^{\sigma_l}$ are right-normalized, respectively.¹²²

In contrast with the CASSCF/CI wavefunction in Eq. (1), for which all the CI coefficients are determined in one step, DMRG optimizes MPS wavefunctions iteratively with one (or two adjacent, see below) \mathbf{M}^{σ_l} MPS tensors at a time, while ensuring that maximum dimensions of these matrices do not exceed a certain value m , which is denoted as the *bond dimension* or *number of renormalized block states*. Due to this systematic dimension reduction, the exponential scaling of Eq. (1) is reduced to polynomial scaling. In analogy to Eq. (21), also operators may be represented as matrix product operators (MPOs):

$$\hat{W} = \sum_{\sigma, \sigma'} \sum_{b_1 \dots b_{L-1}} W_{1b_1}^{\sigma_1 \sigma'_1} W_{b_1 b_2}^{\sigma_2 \sigma'_2} \cdots W_{b_{L-1} 1}^{\sigma_{L-1} \sigma'_{L-1}} |\sigma\rangle \langle \sigma'|. \quad (23)$$

(We shall not go into detail here on how to obtain the MPO representation for various operators: this has been described in detail in our previous work.¹²³)

In that case, the optimization of a MPS wavefunction is formulated as the variational optimization of the entries of a single (or two adjacent) MPS tensors to minimize the expectation value of the energy $E^\Psi = \langle \Psi | \hat{H} | \Psi \rangle$, under the constraint that the wavefunction is normalized:

$$\delta \left(\langle \Psi | \hat{H} | \Psi \rangle - \lambda (\langle \Psi | \Psi \rangle - 1) \right) = 0 \quad (24)$$

Inserting the MPO expression for the Hamiltonian \hat{H} into the expression for the expectation value of the energy, we obtain

$$\mathbb{L}_{a_0 a'_0}^{b_0} = 1 \quad (26)$$

$$\mathbb{L}_{a_1 a'_1}^{b_1} = \sum_{\sigma_1 \sigma'_1} M_{a_1 1}^{\sigma_1 \dagger} W_{1 b_1}^{\sigma_1 \sigma'_1} M_{1 a'_1}^{\sigma'_1}, \quad (27)$$

$$\dots$$

$$\mathbb{L}_{a_l a'_l}^{b_l} = \sum_{\substack{a_{l-1} a'_{l-1} b_{l-1} \\ \sigma_{l-1} \sigma'_{l-1}}} M_{a_l a_{l-1}}^{\sigma_l \dagger} W_{b_{l-1} b_l}^{\sigma_{l-1} \sigma'_l} \mathbb{L}_{a_{l-1} a'_{l-1}}^{b_{l-1}} M_{a'_{l-1} a'_l}^{\sigma'_{l-1}}, \quad (28)$$

and analogously *right boundaries*

$$\mathbb{R}_{a'_{l-1} a_{l-1}}^{b_{l-1}} = \sum_{\substack{a_l a'_l b_{l-1} \\ \sigma_l \sigma'_l}} M_{a'_l a_{l-1}}^{\sigma'_l} W_{b_{l-1} b_l}^{\sigma_l \sigma'_l} \mathbb{R}_{a'_l a_l}^{b_l} M_{a_l a_{l-1}}^{\sigma_l \dagger}. \quad (29)$$

Assuming that the left and right boundaries have been constructed from left- and right-normalized tensors, respectively, inserting the definition of boundaries into Eq. (24) yields an eigenvalue equation $\mathcal{H}v = \lambda v$, where \mathcal{H} is the local Hamiltonian matrix at site l with matrix elements

$$\begin{aligned} \mathcal{H}_{IJ} &= \mathcal{H}_{(a_{l-1} \sigma_l a_l), (a'_{l-1} \sigma'_l a'_l)} = \mathcal{H}_{a_{l-1} a_l a'_{l-1} a'_l}^{\sigma_l \sigma'_l} \\ &= \sum_{b_{l-1} b_l} \mathbb{L}_{a_{l-1} a'_{l-1}}^{b_{l-1}} W_{b_{l-1} b_l}^{\sigma_l \sigma'_l} \mathbb{R}_{a'_l a_l}^{b_l}, \end{aligned} \quad (30)$$

and

$$v_I = M_{(a_{l-1} \sigma_l a_l)} = M_{a_{l-1} a_l}^{\sigma_l}, \quad (31)$$

where we combined one set of indices $(a_{l-1} \sigma_l a_l)$ into one composite index to form the matrix \mathcal{H} and the vector v . After the lowest (or several lowest, see below) eigenvalue(s) λ have been obtained, the corresponding eigenvector(s) are reshaped again into the MPS tensor $M_{a_{l-1} a_l}^{\sigma_l}$. A subsequent normalization and truncation procedure such as singular value decomposition (SVD) ensures that the maximum dimension of $M_{a_{l-1} a_l}^{\sigma_l}$ does not exceed m . A basis transformation finalizes the local optimization at site l , generating a new mixed-canonical form of the MPS at site $l+1$. The process (*sweep*) is repeated until the final site L is reached and then its direction is reversed. In passing, we note that commonly two adjacent MPS tensors are optimised simultaneously (two-site DMRG),⁴³ which is, however, not an important aspect for the purpose of this work. For further details on the DMRG optimization procedure we refer the reader to Refs. 43,122,123.

After optimization of the MPS wavefunction, we can easily obtain one- and two-particle density matrices as expectation values of operators within the MPS-MPO framework of DMRG.^{43,122} This allows us to formulate a (SA-)DMRG-SCF procedure in an analogy with the (SA-)CASSCF procedure, with the CI coefficient optimization step in CASSCF replaced by a DMRG procedure in DMRG-SCF.^{71,75} Importantly, Eqs. (4) and (6) remain the same.

D. Definition of variational parameters for analytical gradients for SA-DMRG-SCF

The straightforward derivation of the state-average gradient for an MPS wavefunction by means of Eqs. (10)-(13) is far from trivial. Unlike the expansion of Eq. (1), the CI coefficients are not explicitly available for a MPS wavefunction. Hence, one must define an analogous set of *MPS parameters* which are equivalent to the CI parameters $\mathbf{c}^1, \mathbf{c}^2, \dots, \mathbf{c}^n$ in Eq. (7).

To obtain such parameters, let us define two auxiliary MPSs in orbital subspaces spanned by sites 1 to $l-1$ and $l+1$ to L :

$$|a_{l-1}\rangle = \sum_{\sigma_1 \dots \sigma_{l-1}, a_1 \dots a_{l-2}} A_{1 a_1}^{\sigma_1} \dots A_{a_{l-2} a_{l-1}}^{\sigma_{l-1}} |\sigma_1 \dots \sigma_{l-1}\rangle \quad (32)$$

$$|a_l\rangle = \sum_{\sigma_{l+1} \dots \sigma_L, a_{l+1} \dots a_L} B_{a_{l+1} a_{l+1}}^{\sigma_{l+1}} \dots B_{a_{L-1} a_{L-1}}^{\sigma_L} |\sigma_{l+1} \dots \sigma_L\rangle. \quad (33)$$

Inserting these equations into the mixed-canonical representation of our MPS at site l (Eq. (22)) yields

$$|\Psi\rangle = \sum_{\sigma_l, a_{l-1}, a_{l+1}} M_{a_{l-1} a_l}^{\sigma_l} |a_{l-1}\rangle \otimes |\sigma_l\rangle \otimes |a_l\rangle \quad (34)$$

where $|\sigma_l\rangle$ is the local basis state for orbital l , corresponding to its four possible occupations: unoccupied, spin-up, spin-down, and doubly occupied. Grouping the indices $(a_{l-1} \sigma_l a_l)$ as in Eqs. (30) and (31), we arrive at an expression for $|\Psi\rangle$ equivalent to Eq. (1):

$$|\Psi\rangle = \sum_I v_I |\Phi_I\rangle \quad (35)$$

(From now on indices I and J in equations containing MPS will refer to the grouped indices $(a_{l-1} \sigma_l a_l)$, in analogy to CI configurations, which are also labelled I in Eq. (1).

Since each optimization of an MPS tensor $M_{a_{l-1} a_l}^{\sigma_l}$ is equivalent to a solution of a CI problem, we may introduce a vector of MPS parameters \mathbf{v}^Ψ for a state Ψ as a solution of the eigenvalue equation with the Hamiltonian of Eq. (30), i.e. a normalized set of numbers which may form, after reshaping, a tensor $M_{a_{l-1} a_l}^{\sigma_l}$. In a similar manner, the CI parameters \mathbf{c}^Ψ in Eq. (7) are solutions to the CI eigenvalue equation. We may now define MPS Lagrange multipliers $\bar{\mathbf{v}}^\Psi$ in analogy to the CI Lagrange multipliers $\bar{\mathbf{c}}^\Psi$ and construct a Lagrangian for a DMRG-SCF wavefunction similarly to Eq. (9) employing MPS Lagrange multipliers.

Such definition of MPS parameters places a constraint on some properties of the MPS. The configuration basis $|\phi_i\rangle$ in Eq. (1) is, by definition, the same for all states in the state-average description. This is not necessarily true for a set of MPS, if they are optimized individually because $|a_{l-1}\rangle$ and $|a_l\rangle$ (Eq. 34) will be different for each

state. Moreover, in this case not even the dimensions of the individual $M_{a_{l-1}a_l}^{\sigma_l}$ may be the same for all states. Consequently, for our definition of MPS parameters to be valid, the basis $|\Phi_i\rangle$ in Eq. (35) must also be *the same for all states in the state-average description*. This can be ensured if all MPS are optimized and brought into a mixed-canonical form simultaneously, where the truncation and the basis transformation step during the sweeps are the same for all states. In practice, this means employing *common left- and right boundaries for all states* by following the procedure described in Ref. 124. We have implemented such a procedure in our new DMRG MPS-MPO solver: the details of the implementation are, however, beyond the scope of this work and will be described in a future publication.

It remains to be specified at which site l we write the MPS in Eq. (22) to define our MPS parameters, as the choice is, in principle, arbitrary. However, the site must be chosen a priori before solving the CP-MCSCF equations. We will call this site the *linear response site* for convenience. At first glance, there should be no difference, because for an optimized MPS wavefunction all mixed canonical forms at all possible linear response sites l are equivalent. However, the number of MPS parameters is not the same for different choices of l : with sites towards the middle of the lattice, the number of parameters grows, and so does the accuracy of the gradient calculation. We will demonstrate this with an example in Section III B. In passing we note that in Ref. 75 we have employed a similar definition of MPS parameters, where, in contrast to this work, i) two-site tensors at the first two sites have been employed in the definition instead of simple one-site MPS tensors at an arbitrary site and ii) the requirement of the same local basis $|\Phi_i\rangle$ for several states was not met. As we will see later in Sec-

tion III B, linear response sites in the middle of a lattice give a greater variational flexibility of the wavefunction compared to the sites at the edge as in Ref. 75. Two-site tensors as in Ref. 75 are also not needed here due to the aforementioned variational flexibility.

E. Implementation of SA-DMRG-SCF analytical gradients

The definition of MPS parameters in Subsection II D and the identification of a local optimization of an MPS tensor $M_{a_{l-1}a_l}^{\sigma_l}$ as CI problem allow us to formulate the SA-DMRG-SCF analytical gradient theory very closely following the SA-CASSCF theory, i.e. by applying Eqs. (10)-(13) to SA-DMRG-SCF wavefunctions (which have been optimized as described in Subsection II D). This has another advantage, namely that we may derive our implementation from an existing SA-CASSCF analytical gradient implementation. In this work, we have based our implementation on the SA-CASSCF analytical gradient implementation in OpenMOLCAS.^{105,125,126} It employs the PCG method to solve the CP-MCSCF equations (13) iteratively, evaluating the Hessian-trial vector products in each iteration.

Below we shall outline the quantities required for the analytical gradient calculation, whose evaluation is specific to the MPS wavefunction.

a. Transition density matrices. Evaluation of transition density matrix elements may be performed with the help of Eq. (25).¹²³ For an MPS

$$|\bar{\Psi}\rangle = \sum_{\sigma} \sum_{a_1 \dots a_{L-1}} \bar{M}_{1a_1}^{\sigma_1} \bar{M}_{a_1 a_2}^{\sigma_2} \dots \bar{M}_{a_{L-1} 1}^{\sigma_L} |\sigma\rangle \quad (36)$$

an expectation value $\langle \Psi | \hat{\mathcal{W}} | \bar{\Psi} \rangle$ may be calculated as

$$\langle \Psi | \hat{\mathcal{W}} | \bar{\Psi} \rangle = \sum_{\substack{a_{L-1} a'_{L-1} b_{L-1} \\ \sigma_L \sigma'_L}} M_{1a_{L-1}}^{\sigma_L \dagger} W_{b_{L-1} 1}^{\sigma_L \sigma'_L} \left(\dots \sum_{\substack{a_1 a'_1 b_1 \\ \sigma_2 \sigma'_2}} M_{a_2 a_1}^{\sigma_2 \dagger} W_{b_1 b_2}^{\sigma_2 \sigma'_2} \left(\sum_{\sigma_1 \sigma'_1} M_{a_1 1}^{\sigma_1 \dagger} W_{1 b_1}^{\sigma_1 \sigma'_1} \bar{M}_{1 a'_1}^{\sigma'_1} \right) \bar{M}_{a'_1 a'_2}^{\sigma'_2} \dots \right) \bar{M}_{a'_{L-1} 1}^{\sigma'_L} \quad (37)$$

To exploit this for the one- and two-particle transition density matrix elements $\gamma_{pq}^{\Psi\bar{\Psi}}$ and $\Gamma_{pqrs}^{\Psi\bar{\Psi}}$, we replace $\hat{\mathcal{W}}$ in Eq. (37) with the MPO form of the operators

$$\sum_{\tau} a_{p\tau}^{\dagger} a_{q\tau} \quad \text{for } \gamma_{pq}^{\Psi\bar{\Psi}}, \quad (38)$$

$$\sum_{\tau\tau'} a_{p\tau}^{\dagger} a_{\tau\tau'}^{\dagger} a_{s\tau'} a_{q\tau} \quad \text{for } \Gamma_{pqrs}^{\Psi\bar{\Psi}} \quad (39)$$

respectively, and evaluate Eq. (37). (For details on obtaining the MPO form of various operators, see Ref. 123).

If the bra and ket in Eq. (37) differ only by a single tensor, then, instead of recalculating the full Eq. (37) for every expectation value one must calculate all contractions for all sites $\neq l$ only once for all expectation values and recalculate only the contractions involving tensors at site l . During the solution of the CP-MCSCF equations,

only the tensor at site l is updated. This can be seen in Eqs. (41) and (72) in the work of Snyder et al.¹⁰⁹, who update the CI coefficients but retain the basis intact; by analogy, we update only the vector v_i in Eq. (35) and therefore only the MPS tensor at site l . Furthermore, in the framework of SA-DMRG-SCF, $|\bar{\Psi}\rangle$ always differs from $|\Psi\rangle$ only by a single tensor, as multiple states are optimized with a common boundary. However, after a complete sweep the differing site is always at the beginning of the lattice. Hence, to bring the MPS into a usable form, we must perform a simultaneous canonization of all states. Details on this procedure are beyond the scope of this work and will be described in a future publication.

b. Sigma vectors. Calculation of Hessian-trial vector products requires calculation of sigma vectors. For a CI wavefunction Eq. (1), a sigma vector is defined as the

left-hand side of the CI eigenvalue equation, i. e.

$$\Sigma_i = \sum_j H_{ij} c_j \quad (40)$$

where H_{ij} is the matrix element of the Hamiltonian. (Note that in contrast to other literature, e. g. Refs. 105, 109, 127 we denote the sigma vector with a capital Σ to avoid confusion with MPS indices σ .) An expression for the sigma vector for MPS wavefunctions is easily obtained from Eqs. (30) and (31)

$$\begin{aligned} \Sigma_{a'_{l-1} a_l} &= \sum_{a'_{l-1} a'_l \sigma'_l} \mathcal{H}_{a_{l-1} a_l a'_{l-1} a'_l}^{\sigma_l \sigma'_l} M_{a'_{l-1} a'_l}^{\sigma'_l} \\ &= \sum_{a'_{l-1} a'_l \sigma'_l} \sum_{b_{l-1} b_l} \mathbb{L}_{a_{l-1} a'_l}^{b_{l-1}} W_{b_{l-1} b_l}^{\sigma_l \sigma'_l} \mathbb{R}_{a'_l a_l}^{b_l} M_{a'_{l-1} a'_l}^{\sigma'_l} \end{aligned} \quad (41)$$

Also in DMRG this equation constitutes the left-hand side of the local eigenvalue equation for the optimization of an MPS tensor, and, as such, belongs to the core part of our DMRG MPS-MPO implementation.¹²³

c. Diagonal of the Local Hamiltonian. Also diagonal elements of the local Hamiltonian $\mathcal{H}_{a_{l-1} a_l a'_{l-1} a'_l}^{\sigma_l \sigma'_l}$ from Eq. (30) are required in our gradient implementation to calculate the preconditioner for the PCG algorithm.

With the above quantities, we may setup the CP-MCSCF equations and evaluate the gradients. We will closely follow the work of Snyder et al.¹⁰⁹ on SA-CASSCF gradients and present here only DMRG-specific steps in order to be as brief as possible.

Equivalently to SA-CASSCF theory, we must set up and solve the CP-DMRG-SCF equations

$$\begin{pmatrix} \mathbf{H}^{\text{OO}} & \mathbf{H}^{\text{CO}} \\ \mathbf{H}^{\text{OC}} & \mathbf{H}^{\text{CC}} \end{pmatrix} \begin{pmatrix} \tilde{\boldsymbol{\kappa}} \\ \tilde{\boldsymbol{v}}^\ominus \end{pmatrix} = - \begin{pmatrix} \mathbf{g}^\ominus \\ 0 \end{pmatrix} \quad (42)$$

where the only difference to Eq. (13) is that the Lagrange CI parameters $\tilde{\boldsymbol{c}}^\ominus$ have been replaced with the MPS parameters $\tilde{\boldsymbol{v}}^\ominus$. As we employ the PCG solver¹⁰⁵ for the CP-DMRG-SCF equations, we must be able to compute the Hessian-trial vector products $\mathbf{H}^{\text{OO}} \tilde{\boldsymbol{\kappa}}^\ominus$, $\mathbf{H}^{\text{CO}} \tilde{\boldsymbol{v}}^\ominus$, $\mathbf{H}^{\text{OC}} \tilde{\boldsymbol{\kappa}}^\ominus$ and $\mathbf{H}^{\text{CC}} \tilde{\boldsymbol{v}}^\ominus$ with $\tilde{\boldsymbol{\kappa}}^\ominus$ and $\tilde{\boldsymbol{v}}^\ominus$ as trial vectors (which become equal to $\tilde{\boldsymbol{\kappa}}$ and $\tilde{\boldsymbol{v}}^\ominus$ at convergence). $\mathbf{H}^{\text{OO}} \tilde{\boldsymbol{\kappa}}^\ominus$ and \mathbf{g}^\ominus are evaluated exactly as for SA-CASSCF (see, e. g., Eqs. (13)-(21) in Snyder et al.¹⁰⁹). To express the remaining Hessian-trial vector products, we introduce the generalized orbital gradient matrix $\mathbf{T}(\Psi, \bar{\Psi})$. This matrix has been introduced first in Snyder et al.¹⁰⁹ (see Eqs. (35)-(37) therein). However, in our implementation we followed Refs. 105,125 and the standard textbook by Helgaker, Jørgensen and Olsen.¹²⁷ The equations for the calculation of the matrix elements $T_{pq}(\Psi, \bar{\Psi})$ as employed in our implementation are provided below:

$$T_{pq}(\Psi, \bar{\Psi}) = 2(F_{pq}(\Psi, \bar{\Psi}) - F_{qp}(\Psi, \bar{\Psi})), \quad (43)$$

where the generalized Fock matrix $F_{pq}(\Psi, \bar{\Psi})$ is calculated as

$$F_{ip}(\Psi, \bar{\Psi}) = 2 ({}^I F_{pi} \delta_{\Psi \bar{\Psi}} + {}^A F_{pi}(\Psi, \bar{\Psi})) \quad (44)$$

if the first index is inactive and the second is arbitrary and as,

$$\begin{aligned} F_{tp}(\Psi, \bar{\Psi}) &= \sum_u {}^I F_{pu} \gamma_{tu}^{\Psi \bar{\Psi}} + Q_{tp} \\ &= \sum_u {}^I F_{pu} \gamma_{tu}^{\Psi \bar{\Psi}} + \sum_{vwx} \Gamma_{tvwx}^{\Psi \bar{\Psi}} (pv|wx) \end{aligned} \quad (45)$$

if the first index is active and the second is arbitrary, and

$$F_{ap}(\Psi, \bar{\Psi}) = 0 \quad (46)$$

if the first index is virtual. ${}^I F_{pq}$ and ${}^A F_{pq}(\Psi, \bar{\Psi})$ are the *inactive* and *active* Fock matrices, respectively:

$${}^I F_{pq} = \langle p|h|q \rangle + \sum_i (2(pq|ii) - (pi|i q)), \quad (47)$$

$${}^A F_{pq}(\Psi, \bar{\Psi}) = \sum_{vw} \gamma_{vw}^{\Psi \bar{\Psi}} \left((pq|vw) - \frac{1}{2}(pw|vq) \right). \quad (48)$$

Eqs. (44)-(48) are generalizations of Eqs. (10.8.27)-(10.8.32) from Ref. 127 to transition density matrices between states Ψ and $\bar{\Psi}$. In particular, the state-specific orbital gradient is obtained with $g_{pq}^\ominus = T_{pq}(\Theta, \Theta)$.

Similarly to Snyder et al.¹⁰⁹, the $\mathbf{H}^{\text{CO}} \tilde{\boldsymbol{v}}^\ominus$ product is evaluated as

$$\left(\sum_{\Psi I} H_{\Psi I, pq}^{\text{CO}} \tilde{v}_{\Psi I}^\ominus \right)_{pq} = \sum_{\Psi} 2\omega_{\Psi} T_{pq}(\Psi, \tilde{\boldsymbol{v}}_{\Psi}^\ominus), \quad (49)$$

where $T_{pq}(\Psi, \tilde{\boldsymbol{v}}_{\Psi}^\ominus)$ indicates a matrix element of the \mathbf{T} matrix calculated for a state $|\Psi\rangle$, where the MPS tensor at the linear response site l has been replaced by the corresponding block of the trial vector of MPS parameters $\tilde{\boldsymbol{v}}_{\Psi}^\ominus$, and an unmodified state $|\Psi\rangle$.

The $\mathbf{H}^{\text{CO}} \tilde{\boldsymbol{\kappa}}^\ominus$ product is evaluated from

$$\left(\sum_{pq} H_{\Psi I, pq}^{\text{CO}} \tilde{\kappa}_{pq}^\ominus \right)_{\Psi I} = 2\omega_{\Psi} \left(\tilde{\Sigma}_I^{\Psi} - \sum_{\Phi} v_I^{\Phi} R^{\Psi \Phi} \right) \quad (50)$$

with

$$R^{\Psi \Phi} = \sum_J \tilde{\Sigma}_J^{\Psi} v_J^{\Phi}. \quad (51)$$

The modified sigma vector $\tilde{\Sigma}_I^{\Psi}$ is evaluated from Eq. (41), where, however, a modified Hamiltonian

$$\hat{H} = \sum_{\substack{t,u \\ \tau}} \langle t|\tilde{h}|u \rangle a_{p\tau}^\dagger a_{q\tau} + \frac{1}{2} \sum_{\substack{t,u,v,w \\ \tau, \tau'}} (tu|\tilde{v}w) a_{t\tau}^\dagger a_{v\tau'}^\dagger a_{w\tau'} a_{u\tau} \quad (52)$$

with transformed integrals¹²⁷

$$\langle t|\tilde{h}|u\rangle = \sum_p \tilde{\kappa}_{tp}^{\Theta I} F_{pu} + \sum_{pq} \tilde{\kappa}_{pq}^{\Theta} (2(pq|tu) - (pt|qu)) \quad (53)$$

and

$$\begin{aligned} (tu|\tilde{v}v) = & \sum_p \left(\tilde{\kappa}_{tp}^{\Theta} (pu|vw) - \tilde{\kappa}_{pu}^{\Theta} (tp|vw) + \right. \\ & \left. + \tilde{\kappa}_{vp}^{\Theta} (tu|pw) - \tilde{\kappa}_{pw}^{\Theta} (tu|vp) \right) \quad (54) \end{aligned}$$

is employed instead of the Hamiltonian in the form of Eq. (2).

We should also note that calculating the $\mathbf{H}^{\text{CO}}\tilde{\kappa}^{\Theta}$ product yields another computational advantage to the calculation of the full Hessian block \mathbf{H}^{CO} (in addition to the obvious advantage of not storing the full Hessian). The calculation of \mathbf{H}^{CO} would require one- and two-particle RDM derivatives with respect to MPS parameters,^{75,111} which we have shown in previous work,⁷⁵ has the cost of an evaluation of a transition density matrix for each single MPS parameter. As the number of MPS parameters may become extremely large, albeit limited by m , the cost of evaluating RDM derivatives would easily become a bottleneck of the calculation. However, calculating $\mathbf{H}^{\text{CO}}\tilde{\kappa}^{\Theta}$ by means of Eq. (50) avoids the calculation of RDM derivatives altogether.

The $\mathbf{H}^{\text{CC}}\tilde{v}^{\Theta}$ product, similarly to the CI case (cf. Eq. (39) in Ref. 109 or Eq. (30) in Ref. 105), is evaluated from

$$\begin{aligned} \left(\sum_{\Phi J} H_{\Psi I, \Phi J}^{\text{CC}} \tilde{v}_{\Phi J}^{\Theta} \right)_{\Psi I} &= 2\omega_{\Psi} \left(\sum_J \mathcal{H}_{IJ} \tilde{v}_{\Psi J}^{\Theta} - E^{\Psi} \tilde{v}_{\Psi I}^{\Theta} \right) \\ &= 2\omega_{\Psi} (\tilde{\Sigma}_I^{\Psi} - E^{\Psi} \tilde{v}_{\Psi I}^{\Theta}). \quad (55) \end{aligned}$$

Here we must again calculate a sigma vector $\tilde{\Sigma}_I^{\Psi}$ with the help of Eq. (41), where, similarly to the Eq. (49), the MPS tensor $\{M_{a_{l-1}a_l}^{\sigma_l}\}$ is replaced with the block of the trial vector of MPS parameters $\tilde{v}_{\Psi}^{\Theta}$, reshaped according to the MPS tensor structure.

After solving the CP-DMRG-SCF equations we obtain a set of the orbital and MPS parameters $\tilde{\kappa}$ and \tilde{v}^{Θ} , which allow us to construct the effective one- and two-particle RDMs from Eqs. (15)-(20). The transition density matrices $\gamma_{pq}^{\Psi\tilde{v}^{\Theta}}$ and $\Gamma_{pqrs}^{\Psi\tilde{v}^{\Theta}}$, analogs of their CI counterparts $\gamma_{pq}^{\Psi\tilde{c}^{\Theta}}$ and $\Gamma_{pqrs}^{\Psi\tilde{c}^{\Theta}}$ from Eqs. (18) and (20), are obtained as in Eq. (49), namely by replacing the MPS tensor $\{M_{a_{l-1}a_l}^{\sigma_l}\}$ in the MPS Ψ at the linear response site l with the block of the trial vector of MPS parameters $\tilde{v}_{\Psi}^{\Theta}$, reshaped accordingly, and evaluating the transition density matrices between the unmodified Ψ and the modified state. Finally, the effective density matrices allow us to construct the Lagrangian in Eq. (9) and evaluate the gradient according to Eq. (14). This is completely identical to the SA-CASSCF procedure and has been described extensively in Refs. 105 and 109.

F. Nonadiabatic couplings

As in the SA-CASSCF case,^{109,128} the calculation of the nonadiabatic couplings for two states Θ and Λ , $\langle \Theta | \partial / \partial x | \Lambda \rangle$, is very similar to the calculation of the gradients, with the following differences:

- The orbital gradient \mathbf{g}^{Θ} in the CP-MCSCF equations (13) or (42) is replaced by the generalized orbital gradient $\mathbf{T}(\Theta, \Lambda)$ with the average being calculated over two different states (Θ and Λ).
- In the expressions for the effective one- and two-particle RDMs (Eqs. (15) and (16)) the state-specific density matrices γ^{Θ} and Γ^{Θ} are replaced by the symmetrized transition density matrices $\gamma^{\Theta\Lambda}$ and $\Gamma^{\Theta\Lambda}$, respectively.
- For calculation of the nonadiabatic couplings from the Lagrangian, Eq. (14) is scaled by $(E_{\Theta} - E_{\Lambda})^{-1}$ and gains an additional term, becoming

$$\begin{aligned} \left\langle \Theta \left| \frac{\partial}{\partial x} \right| \Lambda \right\rangle &= \frac{1}{E_{\Theta} - E_{\Lambda}} \times \\ &\times \left(\sum_{pq} \frac{\partial \langle p|h|q\rangle}{\partial x} \gamma_{pq}^{\Theta,e} + \frac{1}{2} \sum_{pqrs} \frac{\partial \langle pq|rs\rangle}{\partial x} \Gamma_{pqrs}^{\Theta,e} - \right. \\ &\left. - \sum_{pq} X_{pq}^{\Theta,e} \frac{\partial S_{pq}}{\partial x} \right) + \sum_{pq}^{\text{AS}} f_{pq}, \quad (56) \end{aligned}$$

with

$$f_{pq}^{\text{AS}} = -\frac{1}{2} \gamma_{pq}^{\Theta\Lambda, \text{ns}} \left(\left(\frac{\partial \phi_p}{\partial x} | q \right) - (p | \frac{\partial \phi_q}{\partial x}) \right), \quad (57)$$

where f_{pq}^{AS} is the contribution that arises from the antisymmetric transition density matrix $\gamma_{pq}^{\Theta\Lambda, \text{ns}}$ and the antisymmetric derivative overlap $\left(\left(\frac{\partial \phi_p}{\partial x} | q \right) - (p | \frac{\partial \phi_q}{\partial x}) \right)$.¹⁰⁹ In SA-CASSCF nonadiabatic coupling theory, this contribution is termed ‘‘configuration state function (CSF) contribution’’,¹²⁸ however here we prefer not to use this term as we do not operate in CSF basis in DMRG.

III. NUMERICAL EXAMPLES

A. General computational details

In the numerical examples below all SA-CASSCF calculations have been performed with the OpenMOLCAS¹²⁶ software package, and the SA-DMRG-SCF calculations with the development version of the QCMAquis^{123,129} DMRG program and the QCMAquis-OpenMOLCAS interface. In all examples, we have chosen the number of sweeps and the maximum number of renormalized block states m in DMRG-SCF

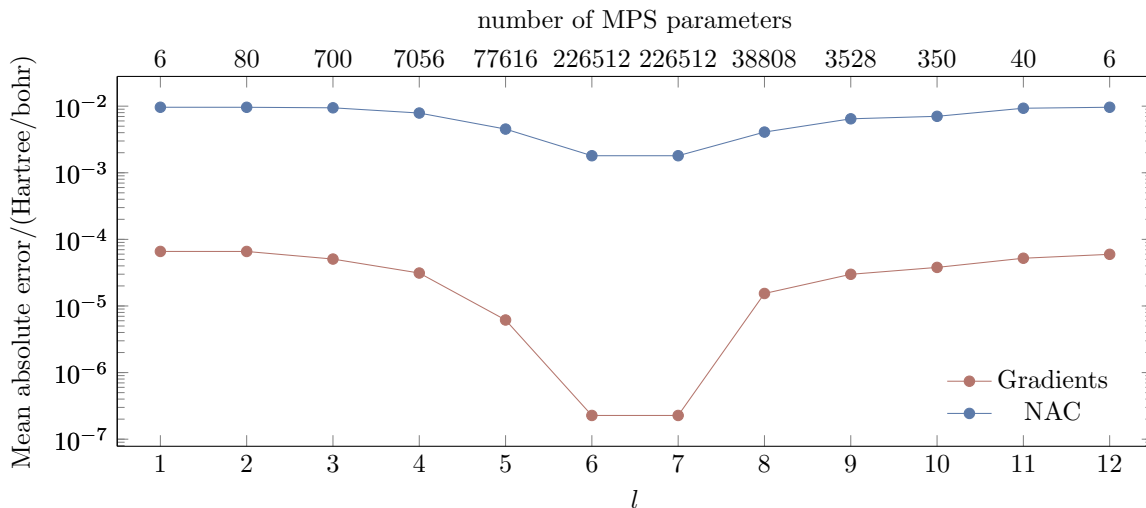


FIG. 1. Mean absolute error (with respect to the SA-CASSCF result) of gradients for the S_1 state and the nonadiabatic couplings (NAC) between the S_0 and S_1 states of cyclobutadiene, calculated with SA-DMRG-SCF(12,12)[2000], for different linear response sites l . The x axis on the top lists the corresponding number of MPS parameters: for $l = 6$ and 7 the number of MPS parameters is equal to the number of the CI coefficients in the reference SA-CASSCF calculation.

to approximate the CASSCF energy to an accuracy of 10^{-8} Hartree. Although DMRG-SCF makes energy and gradient calculations for large active spaces accessible, in this work we restrict ourselves to a problem that can still be treated with the standard CASSCF for the sake of comparison.

For our first example, cyclobutadiene (Section III B), a full-valence active space, consisting of 12 electrons in 12 orbitals, with Dunning’s cc-pVDZ¹³⁰ basis set was chosen. The optimized orbitals in both SA-CASSCF and SA-DMRG-SCF calculations turned out to be identical, as expected, and the maximum number of renormalized block states m in DMRG-SCF was set to 2000.

For our second example, the 1,2-dioxetanone (Section III C), an active space of 16 electrons in 13 orbitals, along with the ANO-RCC-VDZP basis set¹³¹ was employed as suggested in Ref. 132. The maximum number of renormalized block states m was raised to 5000,

Figure 1 shows the mean absolute error of gradients of the S_1 state and the nonadiabatic couplings between the S_0 and S_1 states for various linear response sites, along with the corresponding number of MPS parameters. The mean absolute error is defined as

$$\text{MAE} = \frac{1}{n} \sum_{i=1}^n |g_i^{\text{DMRG-SCF}} - g_i^{\text{CASSCF}}| \quad (58)$$

where $g_i^{\text{DMRG-SCF}}$ and g_i^{CASSCF} are DMRG-SCF and CASSCF gradients or nonadiabatic couplings, respectively, and n is their total number. Both errors clearly show their minimum in the middle of the lattice, where the number of MPS variational parameters of the wavefunction is the largest. Note that here, i.e., for sites 6 and 7, the number of MPS Lagrange multipliers is equal to the number of CI Lagrange multipliers in the

again to reproduce the CASSCF energy to an accuracy of 10^{-8} Hartree.

B. Cyclobutadiene: Dependence of the gradient on the choice of the linear response site

In this subsection we examine how the choice of the linear response site determines the error in gradients and nonadiabatic couplings, with cyclobutadiene as an example. The automerization reaction of cyclobutadiene is the most prominent example of a process primarily driven by heavy-atom tunnelling.^{133–135} As such, it has been subject to ab-initio dynamic simulations,¹³⁶ which necessitate the usage of nuclear gradients. A single molecular structure along the automerization reaction path from Ref. 136 has been chosen for our example below.

CASSCF reference calculations, and therefore one would expect that in case of a perfect match of CASSCF and DMRG-SCF wavefunctions the gradients should also be identical. Still, we observe a small error of approximately 10^{-7} Hartree/bohr, which is attributed to the small numerical differences between CASSCF and DMRG-SCF wavefunctions, caused by nonzero convergence thresholds for the orbital optimization, DMRG sweeps, and the PCG method in CP-DMRG-SCF equations. By tightening the convergence thresholds the error decreases. Consequently, for the subsequent examples, we chose a linear response site in the middle of the lattice for the best accuracy.

With linear response sites towards the edge of the lattice, the gradient error increases by up to three orders of magnitude, as also the variational flexibility of the wavefunction decreases. However, by varying the lin-

ear response site we may trade the gradient accuracy against the computational cost, as CP-DMRG-SCF equations with fewer Lagrange multipliers converge faster. This allows one to provide a good approximation to the DMRG-SCF gradient for cases where no tight convergence is required. The largest variational flexibility, and therefore, potentially the lowest DMRG-SCF gradient error would most likely be obtained with a sweep-like procedure, where CP-DMRG-SCF equations are solved for every site and the nonvariational contributions to the RDMs are obtained at the end of the sweep. Such a procedure is subject of our future work, but we would expect it to have a very high computational cost due to the sweeping procedure. The current algorithm, based on a single linear response site, as we see here, already achieves a very good accuracy at a rather moderate computational cost by solving CP-DMRG-SCF equations only once.

Surprisingly, the nonadiabatic couplings show errors up to four orders of magnitude larger than the gradients. However, the error in nonadiabatic couplings can be attributed to their larger sensitivity to the wavefunction quality in general: in a DMRG-SCF calculation with an extremely tight energy convergence threshold for the sweep of 10^{-12} Hartree the average deviation of the couplings from their SA-CASSCF counterparts could be reduced to 7×10^{-6} Hartree/bohr. The sensitivity of nonadiabatic couplings to the quality of the reference wavefunction is not limited to DMRG-SCF but can be observed between several reference CASSCF calculations: a SA-CASSCF calculation with a lower Davidson diagonalization threshold of 10^{-9} Hartree yields nonadiabatic couplings which differ on average by 1.3×10^{-7} Hartree/bohr from the original CASSCF calculation. Note that these deviations in the nonadiabatic couplings have no practical effect on a conical intersection optimization, as we will see below.

C. 1,2-Dioxetanone: Optimization of a conical intersection

1,2-dioxetanone (Fig. 2a) is a simple chemoluminescent compound, whose thermal dissociation mechanism, along with those of its substituted derivatives have been extensively studied in chemo- and bioluminescence studies.^{132,137–145} Liu et al.¹³² performed an extensive computational study on the dissociation pathway of 1,2-dioxetanone and located two conical intersections between the $\sigma\sigma^*$ and the $n\sigma^*$ states along the pathway. In the vicinity of these conical intersections both states share a significant biradical character, which mandates a multiconfigurational treatment such as CASSCF. We performed an optimization of the first $(\sigma\sigma^*), (n\sigma^*)$ conical intersections along the reaction path, named by Liu et al.¹³² as “ $^1\sigma\sigma^*$ -TS”, both with CASSCF and DMRG-SCF. The optimization run for both methods is presented in Table I. At each step the energies and the gradients are nearly identical, and the discrepan-

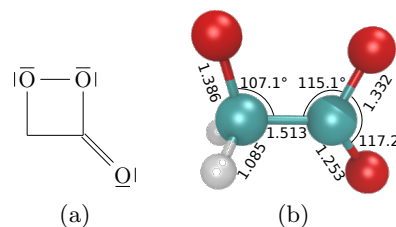


FIG. 2. (a): Lewis structure of 1,2-dioxetanone. (b): $(\sigma\sigma^*), (n\sigma^*)$ -CI (named “ $^1\sigma\sigma^*$ -TS” in Ref. 132) structure optimized in this work with most important bond lengths (in Å) and angles.

cies are very small – below 2.8×10^{-6} Hartree for the energies, 6×10^{-5} Hartree/Bohr for gradient norms and 6.3×10^{-5} Hartree/Bohr for the maximum gradient element – in all cases well below the convergence thresholds for the optimization. These small discrepancies again decrease even further by tightening the convergence thresholds. The optimized structures are also essentially identical for both methods: the maximum absolute difference in the Cartesian coordinates is 2×10^{-4} Å for both optimized structures. The most important bond lengths and angles of the optimized structure are presented in Fig. 2b. As we see, a conical intersection optimization with our SA-DMRG-SCF analytical gradient and nonadiabatic coupling *ansatz* is able to accurately reproduce the SA-CASSCF optimization result.

D. 1,2-Dioxetanone: Gradient convergence with number of renormalized block states

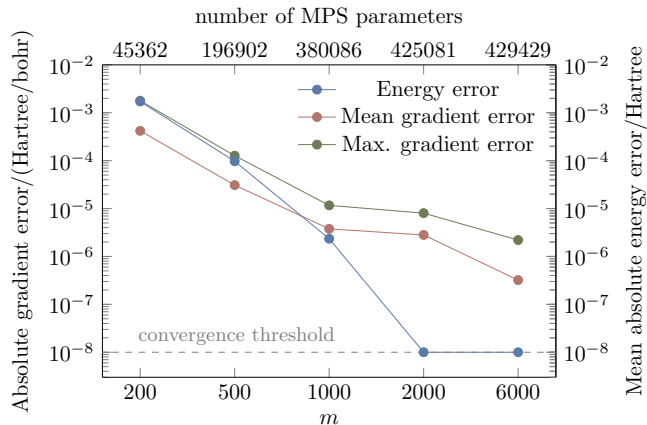


FIG. 3. Mean and maximum absolute errors (with respect to the SA-CASSCF result) of gradients for the S_1 state for 1,2-dioxetanone at the S_0 optimized structure, from SA-DMRG-SCF(16,13) calculations with different values for the number of renormalized block states m . For $m = 6000$, the number of MPS parameters corresponds to that of the reference SA-CASSCF calculation. The average error for the energies of S_0 and S_1 states is shown for comparison.

Having established that our SA-DMRG-SCF gradient *ansatz* is able to reproduce SA-CASSCF gradients to an accuracy that is only dependent on convergence thresholds in cases where an m value is sufficiently large to reproduce the SA-CASSCF wavefunction to arbitrary accuracy, we now study the gradient error for smaller m values, i. e., when the approximation of the SA-CASSCF wavefunction by a SA-DMRG-SCF wavefunction is of a reduced quality. For this, a gradient calculation has been performed for the S_0 optimized structure (i. e. the starting structure for the optimization in Section III C) with SA-DMRG-SCF(16,13), but with several m values varying from 200 to 6000.

Fig. 3 shows the mean and maximum absolute gradient error for each m , along with the average energy error. We recognize that for large m values ($m \geq 2000$), the gradient error is one to two orders of magnitude larger than the energy error, and that an m value which is sufficient to converge the energy up to an error of 10^{-8} Hartree is not sufficient to converge the gradient to the same accuracy as the energy. Even a much larger value ($m = 6000$) does not converge the gradient to the same accuracy, although the error decreases by another order of magnitude. We

expect that tightening the convergence threshold for the energy along with larger m values would improve the convergence even further. However (as we see both from this result and the conical intersection optimization in the previous section) even at $m = 2000$, the gradient error is well below typical convergence thresholds for optimizations and can therefore be neglected for practical applications.

However, for small m values we see an interesting development: although the maximum gradient error is approximately the same or larger than the energy error, the mean gradient error is actually smaller. The crossover of the mean energy and gradient errors occurs around $m = 1000$. While we believe that this result is caused by a fortitious error cancellation, it implies that for typical DMRG-SCF calculations, which are performed for active spaces inaccessible by standard CASSCF the accuracy of the gradient error is of the same order of magnitude or smaller than the energy error. In other words, in these calculations we may extract energies and gradients of a similar accuracy from the same wavefunction without further refinements such as imposing tighter convergence thresholds.

TABLE I. Average electronic energy, gradient norm, and the maximum gradient element throughout the $(\sigma\sigma^*), (n\sigma^*)$ conical intersection optimization in 1,2-dioxetanone.

Step	Electronic energy/ Hartree		Avg. gradient norm/ Hartree/bohr		Max. gradient element/ Hartree/bohr	
	CASSCF	DMRG-SCF	CASSCF	DMRG-SCF	CASSCF	DMRG-SCF
1	-301.76392482	-301.76392481	0.098030	0.098090	-0.070811	-0.070874
2	-301.77670336	-301.77670325	0.089606	0.089626	-0.050384	-0.050435
3	-301.79392062	-301.79391779	0.159354	0.159318	0.127371	0.127362
4	-301.78862423	-301.78862694	0.073202	0.073216	-0.034099	-0.034124
5	-301.81089953	-301.81089903	0.066443	0.066451	0.037325	0.037307
6	-301.81982062	-301.81982236	0.027812	0.027800	-0.017275	-0.017280
7	-301.82254958	-301.82254963	0.017071	0.017075	0.012606	0.012609
8	-301.82398804	-301.82398842	0.011692	0.011693	-0.008136	-0.008114
9	-301.82423076	-301.82423099	0.004222	0.004204	-0.003256	-0.003232
10	-301.82426240	-301.82426246	0.000897	0.000897	-0.000552	-0.000549
11	-301.82426314	-301.82426325	0.000404	0.000387	-0.000269	-0.000254

IV. CONCLUSIONS

In this paper, we presented for the first time the implementation of a Lagrangian-based *ansatz* for the analytical state-average DMRG-SCF gradients and nonadiabatic couplings which requires construction and solution of CP-MCSCF equations. Our *ansatz* generalizes the SA-CASSCF gradients theory first presented by Stålring et al.¹⁰⁵ in 2001 to wavefunctions encoded as MPSs. We derive the Lagrange multipliers in the CP-MCSCF equations from the mixed-canonical representation of the MPS wavefunction at one particular site, here called the linear response site, which can be chosen arbitrarily. The choice of the linear response site can be made a tradeoff

between accuracy and computational cost. We further argue that for the validity of our definition of MPS Lagrange multipliers the MPS for all states must be optimized simultaneously with common left and right boundaries. Finally, we showed that our SA-DMRG-SCF gradient and nonadiabatic coupling *ansatz* will exactly reproduce SA-CASSCF gradients and nonadiabatic couplings, respectively, if the SA-DMRG-SCF wavefunction reproduces the SA-CASSCF wavefunction exactly. If this is not the case, both gradients and, in particular, nonadiabatic couplings show errors that are larger than the errors in energy. We have demonstrated the feasibility of our method in practical applications by performing a conical intersection optimization of 1,2-dioxetanone, reproducing

the result of a SA-CASSCF conical intersection optimization. Our development, in addition to applications for conical intersection optimization for systems with large active spaces, paves the way for surface hopping studies and other excited state studies with DMRG.

ACKNOWLEDGMENTS

L.F. acknowledges the Austrian Science Fund for a Schrödinger fellowship (Project No. J 3935). This work was supported by the Schweizerischer Nationalfonds (SNF project 200021-182400), National Natural Science Foundation of China (NO. 21703260) and Informatization Program of the Chinese Academy of Sciences (NO. XXH13506-403). We thank Prof. Roland Lindh and Dr. Christopher Stein for fruitful discussions.

REFERENCES

- ¹Pierloot, K. In *Theoretical and Computational Chemistry*; Olivucci, M., Ed.; Computational Photochemistry; Elsevier, 2005; Vol. 16; pp 279–315.
- ²Neese, F.; Petrenko, T.; Ganyushin, D.; Olbrich, G. *Coord. Chem. Rev.* **2007**, *251*, 288–327.
- ³Gagliardi, L. In *Reviews in Computational Chemistry*; Lipkowitz, K. B., Cundari, T. R., Eds.; John Wiley & Sons, Inc., 2007; pp 249–284.
- ⁴Neese, F.; Liakos, D. G.; Ye, S. *J. Biol. Inorg. Chem.* **2011**, *16*, 821–829.
- ⁵Pierloot, K. *Int. J. Quantum Chem.* **2011**, *111*, 3291–3301.
- ⁶Daniel, C. *Coord. Chem. Rev.* **2015**, *282–283*, 19–32.
- ⁷Ashley, D. C.; Jakubikova, E. *Coord. Chem. Rev.* **2017**, *337*, 97–111.
- ⁸Radoń, M. *Phys. Chem. Chem. Phys.* **2019**, *21*, 4854–4870.
- ⁹Vogiatzis, K. D.; Polynski, M. V.; Kirkland, J. K.; Townsend, J.; Hashemi, A.; Liu, C.; Pidko, E. A. *Chem. Rev.* **2019**, *119*, 2453–2523.
- ¹⁰González, L.; Escudero, D.; Serrano-Andrés, L. *ChemPhysChem* **2012**, *13*, 28–51.
- ¹¹Plasser, F.; Barbatti, M.; Aquino, A. J. A.; Lischka, H. *Theor. Chem. Acc.* **2012**, *131*, 1–14.
- ¹²Ghosh, S.; Verma, P.; Cramer, C. J.; Gagliardi, L.; Truhlar, D. G. *Chem. Rev.* **2018**, *118*, 7249–7292.
- ¹³Lischka, H.; Nachtigallová, D.; Aquino, A. J. A.; Szalay, P. G.; Plasser, F.; Machado, F. B. C.; Barbatti, M. *Chem. Rev.* **2018**, *118*, 7293–7361.
- ¹⁴Serrano-Andrés, L.; Merchán, M. **2009**, *10*, 21–32.
- ¹⁵Middleton, C. T.; de La Harpe, K.; Su, C.; Law, Y. K.; Crespo-Hernández, C. E.; Kohler, B. *Annu. Rev. Phys. Chem.* **2009**, *60*, 217–239.
- ¹⁶Mai, S.; Richter, M.; Marquetand, P.; González, L. *Top. Curr. Chem.* **2015**, 99–154.
- ¹⁷Gust, D.; Moore, T. A.; Moore, A. L. *Acc. Chem. Res.* **2009**, *42*, 1890–1898.
- ¹⁸Gust, D.; Moore, T. A.; Moore, A. L. *Faraday Discuss.* **2012**, *155*, 9–26.
- ¹⁹Jäger, M.; Freitag, L.; González, L. *Coord. Chem. Rev.* **2015**, *304–305*, 146–165.
- ²⁰Agbe, H.; Nyankson, E.; Raza, N.; Dodoo-Arhin, D.; Chauhan, A.; Osei, G.; Kumar, V.; Kim, K.-H. *J. Ind. Eng. Chem.* **2019**, *72*, 31–49.
- ²¹Dolmans, D. E. J. G. J.; Fukumura, D.; Jain, R. K. *Nat. Rev. Cancer* **2003**, *3*, 380–387.
- ²²Rose, M. J.; Mascharak, P. K. *Curr. Opin. Chem. Biol.* **2008**, *12*, 238–244.
- ²³Ormond, A. B.; Freeman, H. S. *Materials* **2013**, *6*, 817–840.
- ²⁴Mehraban, N.; Freeman, H. S. *Materials* **2015**, *8*, 4421–4456.
- ²⁵Roos, B. O.; Taylor, P. R.; Siegbahn, P. E. *Chem. Phys.* **1980**, *48*, 157–173.
- ²⁶Siegbahn, P. E.; Almlöf, J.; Heiberg, A.; Roos, B. O. *J. Chem. Phys.* **1981**, *74*, 2384–2396.
- ²⁷Shepard, R. *Adv. Chem. Phys.* **1987**, *67*, 63–200.
- ²⁸Olsen, J. *Int. J. Quantum Chem.* **2011**, *111*, 3267–3272.
- ²⁹Aquilante, F. et al. *J. Comput. Chem.* **2016**, *37*, 506–541.
- ³⁰Vogiatzis, K. D.; Ma, D.; Olsen, J.; Gagliardi, L.; de Jong, W. A. *J. Chem. Phys.* **2017**, *147*, 184111.
- ³¹White, S. R.; Martin, R. L. *J. Chem. Phys.* **1998**, *110*, 4127–4130.
- ³²Mitrushenkov, A. O.; Fano, G.; Ortolani, F.; Linguerri, R.; Palmieri, P. *J. Chem. Phys.* **2001**, *115*, 6815–6821.
- ³³Chan, G. K.-L.; Head-Gordon, M. *J. Chem. Phys.* **2002**, *116*, 4462–4476.
- ³⁴Legeza, Ö.; Röder, J.; Hess, B. *Phys. Rev. B* **2003**, *67*, 125114.
- ³⁵Chan, G. K.-L. *J. Chem. Phys.* **2004**, *120*, 3172–3178.
- ³⁶Moritz, G.; Hess, B. A.; Reiher, M. *J. Chem. Phys.* **2005**, *122*, 024107.
- ³⁷Moritz, G.; Wolf, A.; Reiher, M. *J. Chem. Phys.* **2005**, *123*, 184105.
- ³⁸Rissler, J.; Noack, R. M.; White, S. R. *Chem. Phys.* **2006**, *323*, 519–531.
- ³⁹McCulloch, I. P. *J. Stat. Mech-Theory E.* **2007**, *2007*, P10014.
- ⁴⁰Legeza, Ö.; Noack, R. M.; Solyom, J.; Tincani, L. Applications of quantum information in the density-matrix renormalization group. *Computational Many-Particle Physics*. 2008; pp 653–664.
- ⁴¹Chan, G. K.-L.; Zgid, D. *Ann. Rep. Comput. Chem.* **2009**, *5*, 149–162.
- ⁴²Marti, K. H.; Reiher, M. *Z. Phys. Chem.* **2010**, *224*, 583–599.
- ⁴³Schollwöck, U. *Ann. Phys.* **2011**, *326*, 96–192.
- ⁴⁴Chan, G. K.-L.; Sharma, S. *Ann. Rev. Phys. Chem.* **2011**, *62*, 465–481.
- ⁴⁵Kurashige, Y.; Yanai, T. *J. Chem. Phys.* **2009**, *130*, 234114.
- ⁴⁶Knecht, S.; Örs Legeza; Reiher, M. *J. Chem. Phys.* **2014**, *140*, 041101.
- ⁴⁷Wouters, S.; van Neck, D. *Eur. Phys. J. D* **2014**, *68*, 272.
- ⁴⁸Yanai, T.; Kurashige, Y.; Mizukami, W.; Chalupský, J.; Lan, T. N.; Saitow, M. *Int. J. Quantum Chem.* **2015**, *115*, 283–299.
- ⁴⁹Knecht, S.; Hedegård, E. D.; Keller, S.; Kovyrshin, A.; Ma, Y.; Muolo, A.; Stein, C. J.; Reiher, M. *Chimia* **2016**, *70*, 244–251.
- ⁵⁰Chan, G. K.; Keselman, A.; Nakatani, N.; Li, Z.; White, S. R. *J. Chem. Phys.* **2016**, *145*, 2863–2865.
- ⁵¹White, S. R. *Phys. Rev. Lett.* **1992**, *69*, 2863.
- ⁵²White, S. R.; Noack, R. *Phys. Rev. Lett.* **1992**, *68*, 3487.
- ⁵³White, S. R.; Martin, R. L. *J. Chem. Phys.* **1999**, *110*, 4127–4130.
- ⁵⁴Daul, S.; Ciofini, I.; Daul, C.; White, S. R. *Int. J. Quantum Chem.* **2000**, *79*, 331–342.
- ⁵⁵Mitrushenkov, A. O.; Fano, G.; Ortolani, F.; Linguerri, R.; Palmieri, P. *J. Chem. Phys.* **2001**, *115*, 6815–6821.
- ⁵⁶Mitrushenkov, A. O.; Linguerri, R.; Palmieri, P.; Fano, G. *J. Chem. Phys.* **2003**, *119*, 4148–4158.
- ⁵⁷Mitrushchenkov, A. O.; Fano, G.; Linguerri, R.; Palmieri, P. *Int. J. Quantum Chem.* **2011**, *112*, 1606–1619.
- ⁵⁸Chan, G. K.-L.; Head-Gordon, M. *J. Chem. Phys.* **2002**, *116*, 4462–4476.
- ⁵⁹Chan, G. K.-L.; Head-Gordon, M. *J. Chem. Phys.* **2003**, *118*, 8551–8554.
- ⁶⁰Chan, G. K.-L. *J. Chem. Phys.* **2004**, *120*, 3172–3178.
- ⁶¹Chan, G. K.-L.; Kállay, M.; Gauss, J. *J. Chem. Phys.* **2004**, *121*, 6110–6116.
- ⁶²Chan, G. K.-L.; Van Voorhis, T. *J. Chem. Phys.* **2005**, *122*, 204101.

- ⁶³Legeza, Ö.; Röder, J.; Hess, B. A. *Mol. Phys.* **2003**, *101*, 2019–2028.
- ⁶⁴Moritz, G.; Hess, B. A.; Reiher, M. *J. Chem. Phys.* **2005**, *122*, 024107.
- ⁶⁵Moritz, G.; Wolf, A.; Reiher, M. *J. Chem. Phys.* **2005**, *123*, 184105.
- ⁶⁶Hachmann, J.; Dorando, J. J.; Avilés, M.; Chan, G. K.-L. *J. Chem. Phys.* **2007**, *127*, 134309.
- ⁶⁷Zgid, D.; Nooijen, M. *J. Chem. Phys.* **2008**, *128*, 014107.
- ⁶⁸Zgid, D.; Nooijen, M. *J. Chem. Phys.* **2008**, *128*, 144116.
- ⁶⁹Zgid, D.; Nooijen, M. *J. Chem. Phys.* **2008**, *128*, 144115.
- ⁷⁰Kurashige, Y.; Yanai, T. *J. Chem. Phys.* **2009**, *130*, 234114.
- ⁷¹Zgid, D.; Nooijen, M. *J. Chem. Phys.* **2008**, *128*, 144116.
- ⁷²Ghosh, D.; Hachmann, J.; Yanai, T.; Chan, G. K.-L. *J. Chem. Phys.* **2008**, *128*, 144117.
- ⁷³Sun, Q.; Yang, J.; Chan, G. K.-L. *Chem. Phys. Lett.* **2017**, *683*, 291–299.
- ⁷⁴Wouters, S.; Bogaerts, T.; Der Voort, P. V.; Van Speybroeck, V.; Van Neck, D. *J. Chem. Phys.* **2014**, *140*, 241103.
- ⁷⁵Ma, Y.; Knecht, S.; Keller, S.; Reiher, M. *J. Chem. Theory Comput.* **2017**, *13*, 2533–2549.
- ⁷⁶Östlund, S.; Rommer, S. *Phys. Rev. Lett.* **1995**, *75*, 3537–3540.
- ⁷⁷Rommer, S.; Östlund, S. *Phys. Rev. B* **1997**, *55*, 2164–2181.
- ⁷⁸Chan, G. K.-L.; Zgid, D. In *Annual Reports in Computational Chemistry*; Wheeler, R. A., Ed.; Elsevier, 2009; Vol. 5; pp 149–162.
- ⁷⁹Mizukami, W.; Kurashige, Y.; Yanai, T. *J. Chem. Theory Comput.* **2012**, *9*, 401–407.
- ⁸⁰Kurashige, Y.; Chan, G. K.-L.; Yanai, T. *Nat. Chem.* **2013**, *5*, 660–666.
- ⁸¹Chalupský, J.; Rokob, T. A.; Kurashige, Y.; Yanai, T.; Solomon, E. I.; Rulíšek, L.; Srnc, M. *J. Am. Chem. Soc.* **2014**, *136*, 15977–15991.
- ⁸²Sharma, S.; Sivalingam, K.; Neese, F.; Chan, G. K.-L. *Nat. Chem.* **2014**, *6*, 927–933.
- ⁸³Yanai, T.; Kurashige, Y.; Mizukami, W.; Chalupsky, J.; Lan, T. N.; Saitow, M. *Int. J. Quantum Chem.* **2015**, *115*, 283–299.
- ⁸⁴Freitag, L.; Knecht, S.; Keller, S.; Delcey, M. G.; Aquilante, F.; Pedersen, T. B.; Lindh, R.; Reiher, M.; Gonzalez, L. *Phys. Chem. Chem. Phys.* **2015**, *17*, 14383–14392.
- ⁸⁵Olivares-Amaya, R.; Hu, W.; Nakatani, N.; Sharma, S.; Yang, J.; Chan, K. L. *J. Chem. Phys.* **2015**, *142*, 034102.
- ⁸⁶Wouters, S.; Van Neck, D. *Eur. Phys. J. D* **2014**, *68*, 272.
- ⁸⁷Pulay, P. *Mol. Phys.* **1969**, *17*, 197–204.
- ⁸⁸Pulay, P. In *Applications of Electronic Structure Theory*; Schaefer, H. F., Ed.; Modern Theoretical Chemistry; Springer US, 1977; pp 153–185.
- ⁸⁹Pulay, P.; Fogarasi, G.; Pang, F.; Boggs, J. E. *J. Am. Chem. Soc.* **1979**, *101*, 2550–2560.
- ⁹⁰Pulay, P. *Theoret. Chim. Acta* **1979**, *50*, 299–312.
- ⁹¹Lengsfeld III, B. H.; Saxe, P.; Yarkony, D. R. *J. Chem. Phys.* **1984**, *81*, 4549–4553.
- ⁹²Hellmann, H. *Einführung in die Quantenchemie*; Leipzig: Deuticke, 1937.
- ⁹³Feynman, R. P. *Phys. Rev.* **1939**, *56*, 340–343.
- ⁹⁴Taylor, P. R. *J. Comput. Chem.* **1984**, *5*, 589–597.
- ⁹⁵Liu, F.; Kurashige, Y.; Yanai, T.; Morokuma, K. *J. Chem. Theory Comput.* **2013**, *9*, 4462–4469.
- ⁹⁶Hu, W.; Chan, K. L. *J. Chem. Theory Comput.* **2015**, *11*, 3000–3009.
- ⁹⁷Nakatani, N.; Guo, S. *J. Chem. Phys.* **2017**, *146*, 094102.
- ⁹⁸Ma, Y.; Knecht, S.; Reiher, M. *ChemPhysChem* **2017**, *18*, 384–393.
- ⁹⁹Yarkony, D. R. *Modern Electronic Structure Theory*; Advanced Series in Physical Chemistry; World Scientific Publishing Company, 1995; pp 642–721.
- ¹⁰⁰Schmidt, M. W.; Gordon, M. S. *Annu. Rev. Phys. Chem.* **2003**, *49*, 233–266.
- ¹⁰¹Docken, K. K.; Hinze, J. *J. Chem. Phys.* **1972**, *57*, 4928–4936.
- ¹⁰²Werner, H.-J.; Meyer, W. *J. Chem. Phys.* **1981**, *74*, 5794–5801.
- ¹⁰³Diffenderfer, R. N.; Yarkony, D. R. *J. Phys. Chem.* **1982**, *86*, 5098–5105.
- ¹⁰⁴Helgaker, T.; Jørgensen, P. *Theor. Chem. Acc.* **1989**, *75*, 111–127.
- ¹⁰⁵Stålring, J.; Bernhardsson, A.; Lindh, R. *Mol. Phys.* **2001**, *99*, 103–114.
- ¹⁰⁶Dupuis, M. *J. Chem. Phys.* **1981**, *74*, 5758–5765.
- ¹⁰⁷Osamura, Y.; Yamaguchi, Y.; Schaefer, H. F. *J. Chem. Phys.* **1982**, *77*, 383–390.
- ¹⁰⁸Snyder, J. W.; Hohenstein, E. G.; Luehr, N.; Martínez, T. J. *J. Chem. Phys.* **2015**, *143*, 154107.
- ¹⁰⁹Snyder, J. W.; Fales, B. S.; Hohenstein, E. G.; Levine, B. G.; Martínez, T. J. *J. Chem. Phys.* **2017**, *146*, 174113.
- ¹¹⁰Lengsfeld, B. H.; Yarkony, D. R. *Adv. Chem. Phys.* **2007**, *1*–71.
- ¹¹¹Werner, H.-J.; Meyer, W. *J. Chem. Phys.* **1980**, *73*, 2342–2356.
- ¹¹²Werner, H.-J.; Knowles, P. J. *J. Chem. Phys.* **1985**, *82*, 5053–5063.
- ¹¹³Knowles, P. J.; Werner, H.-J. *Chem. Phys. Lett.* **1985**, *115*, 259–267.
- ¹¹⁴Werner, H.-J. *Adv. Chem. Phys.* **1987**, *69*, 1–62.
- ¹¹⁵Lengsfeld III, B. H.; Liu, B. *J. Chem. Phys.* **1981**, *75*, 478–480.
- ¹¹⁶Lengsfeld III, B. H. *J. Chem. Phys.* **1982**, *77*, 4073–4083.
- ¹¹⁷Jørgensen, P.; Olsen, J.; Yeager, D. L. *J. Chem. Phys.* **1981**, *75*, 5802–5815.
- ¹¹⁸Yeager, D. L.; Lynch, D.; Nichols, J.; Jørgensen, P.; Olsen, J. *J. Phys. Chem.* **1982**, *86*, 2140–2153.
- ¹¹⁹Olsen, J.; Yeager, D. L.; Jørgensen, P. In *Advances in Chemical Physics*; Prigogine, I., Rice, S. A., Eds.; John Wiley & Sons, Inc., 1983; pp 1–176.
- ¹²⁰Roos, B. O.; Taylor, P. R.; Siegbahn, P. E. *Chem. Phys.* **1980**, *48*, 157–173.
- ¹²¹Szalay, P. G.; Müller, T.; Gidofalvi, G.; Lischka, H.; Shepard, R. *Chem. Rev.* **2011**, *112*, 108–181.
- ¹²²Schollwöck, U. *Phil. Trans. R. Soc. A* **2011**, *369*, 2643–2661.
- ¹²³Keller, S.; Dolfi, M.; Troyer, M.; Reiher, M. *J. Chem. Phys.* **2015**, *143*, 244118.
- ¹²⁴Dolgov, S. V.; Khoromskij, B. N.; Oseledets, I. V.; Savostyanov, D. V. *Comput. Phys. Commun.* **2014**, *185*, 1207–1216.
- ¹²⁵Bernhardsson, A.; Lindh, R.; Olsen, J.; Fülcher, M. *Mol. Phys.* **1999**, *96*, 617–628.
- ¹²⁶<https://gitlab.com/Molcas/OpenMolcas> (accessed 3.5.2019).
- ¹²⁷Helgaker, T.; Jørgensen, P.; Olsen, J. *Molecular electronic-structure theory*; John Wiley & Sons, 2014.
- ¹²⁸Fdez. Galván, I.; Delcey, M. G.; Pedersen, T. B.; Aquilante, F.; Lindh, R. *J. Chem. Theory Comput.* **2016**, *12*, 3636–3653.
- ¹²⁹Keller, S.; Reiher, M. *J. Chem. Phys.* **2016**, *144*, 134101.
- ¹³⁰Dunning Jr, T. H. *J. Chem. Phys.* **1989**, *90*, 1007–1023.
- ¹³¹Roos, B. O.; Lindh, R.; Malmqvist, P.-A.; Veryazov, V.; Widmark, P.-O. *J. Phys. Chem. A* **2005**, *109*, 6575–6579.
- ¹³²Liu, F.; Liu, Y.; De Vico, L.; Lindh, R. *J. Am. Chem. Soc.* **2009**, *131*, 6181–6188.
- ¹³³Carpenter, B. K. *J. Am. Chem. Soc.* **1983**, *105*, 1700–1701.
- ¹³⁴Čársky, P.; Michl, J. *Theoret. Chim. Acta* **1992**, *84*, 125–133.
- ¹³⁵Schoonmaker, R.; Lancaster, T.; Clark, S. J. *J. Chem. Phys.* **2018**, *148*, 104109.
- ¹³⁶Eckert-Maksić, M.; Vazdar, M.; Barbatti, M.; Lischka, H.; Maksić, Z. B. *J. Chem. Phys.* **2006**, *125*, 064310.
- ¹³⁷Schmidt, S. P.; Schuster, G. B. *J. Am. Chem. Soc.* **1978**, *100*, 5559–5561.
- ¹³⁸Adam, W.; Cueto, O. *J. Am. Chem. Soc.* **1979**, *101*, 6511–6515.
- ¹³⁹Turro, N. J.; Chow, M.-F. *J. Am. Chem. Soc.* **1980**, *102*, 5058–5064.
- ¹⁴⁰Liu, F.; Liu, Y.; Vico, L. D.; Lindh, R. *Chem. Phys. Lett.* **2009**, *484*, 69–75.
- ¹⁴¹Navizet, I.; Liu, Y.-J.; Ferré, N.; Roca-Sanjuán, D.; Lindh, R. **2011**, *12*, 3064–3076.
- ¹⁴²Yue, L.; Lan, Z.; Liu, Y.-J. *J. Phys. Chem. Lett.* **2015**, *6*, 540–548.

- ¹⁴³Farahani, P.; Oliveira, M. A.; Fdez. Galván, I.; Baader, W. J. *RSC Adv.* **2017**, *7*, 17462–17472.
- ¹⁴⁴Vacher, M.; Fdez. Galván, I.; Ding, B.-W.; Schramm, S.; Berraud-Pache, R.; Naumov, P.; Ferré, N.; Liu, Y.-J.; Navizet, I.; Roca-Sanjuán, D.; Baader, W. J.; Lindh, R. *Chem. Rev.* **2018**, *118*, 6927–6974.
- ¹⁴⁵Yue, L.; Liu, Y.-J. *J. Chem. Theory Comput.* **2019**, *15*, 1798–1805.